Dynamic Response of Poroelastic Moderately Thick Shells of Revolution Saturated in Viscous Fluid*

Shigeo TAKEZONO**, Katsumi TAO**
and Takeshi GONDA**

This paper describes an analytical formulation and a numerical solution of the elastic dynamic problems of fluid-saturated porous moderately thick shells of revolution. The equations of motion and relations between the strains and displacements are derived from the Reissner-Naghdi shell theory. As the constitutive relations, the consolidation theory of Biot for models of fluid-solid mixtures is employed. The fundamental equations derived are numerically solved by the finite difference method. As a numerical example, the simply supported cylindrical shell under a semi-sinusoidal internal load with respect to time is analyzed, and the variations of pore pressure, displacements and internal forces with time are discussed.

Key Words: Structural Analysis, Numerical Analysis, Finite Difference Method, Dynamic Problems, Poroelastic Shells, Viscous Fluid, Thick Shells

1. Introduction

Porous materials, such as filter materials made of sintering metals, lagging materials, fireproof materials, are utilized for various fields. Furthermore, biological structures, such as hearts, blood vessels, diaphragms can be frequently treated as fluid-saturated poroelastic bodies. In such a fluid-saturated open-cell form, pore fluid flows due to pore pressure gradient, and under the influence of fluid viscosity the higher the deformation rate of the body is, the greater strain rate dependency appears. Jayaraman[1], Okuno and Kingsbury[2], Taber[3],[4] and Kurashige et al.[5],[6] have studied fluid-saturated poroelastic plates, cylinders and cylindrical shells subjected to time dependent surface loads. The authors[7],[8] also have dealt with dynamical problems of axisymmetrical thin shells made of porous materials. From the obtained results, remarkable influence of saturated fluid pressure upon the deformations and internal forces of shells has been recognized in the high loading rate regions.

In the present paper the authors study the dynamic response of fluid-saturated porous moderately thick shells of revolution, considering the effect of shear deformation. The equations of motion derived from the Reissner-Naghdi shell theory[9],[10] for moderately thick shells ($1/20 < h/R < 1/5$; h being the thickness and R being the radius of curvature of the shell) by adding the inertia terms are used. As the constitutive relations for a fluid-saturated poroelastic solid, Biot's consolidation theory[11],[12] is used, and Darcy's law is employed for the viscous fluid flow through a porous elastic solid. In the numerical analysis of the fundamental equations, an usual finite difference form is employed for the spatial derivatives, and the inertia terms are treated with the backward difference formula proposed by Houbolt[13].

As a numerical example, simply supported porous cylindrical shell under the semi-sinusoidal internal pressure with respect to time is analyzed. The difference between the influence of permeability and impermeability on the inner and outer surfaces of the

* Received 15th April, 2002. Japanese original: Trans. Jpn. Soc. Mech. Eng., Vol. 67, No. 653, A (2001), pp. 134-141 (Received 28th April, 2000)

** Department of Mechanical Engineering, Toyohashi University of Technology, Tempaku-cho, Toyohashi 441-8580, Japan. E-mail: tao@mech.tut.ac.jp

shell upon the variations of displacements and internal forces with time is discussed. The results are also compared with those from the Sanders theory[14] for thin shells which neglects the effect of shear deformations.

2. Fundamental Equations

If the middle surface of axisymmetrical shells is given by $R=R(s)$, where R is the distance from the axis and s is the meridional distance measured from a boundary along the middle surface, the relations among the nondimensional curvatures $\omega_\xi(=a/R_s)$, $\omega_\theta(=a/R_\theta)$ and the nondimensional radius $r(=R/a)$ become

$$\left.\begin{aligned}&\omega_\xi=-(\gamma'+\gamma^2)/\omega_\theta,\ \omega_\theta=\sqrt{1-(r')^2}/r,\\&\omega_\theta'=\gamma(\omega_\xi-\omega_\theta),\ r''/r=-\omega_\xi\omega_\theta,\\&\gamma=r'/r,\ \xi=s/a,\ (\ \ )'=d(\ \ )/d\xi,\end{aligned}\right\}\qquad(1)$$

where a is the reference length. An arbitrary point in the shell can be expressed in the orthogonal coordinate system (ξ,θ,ζ) as shown in Fig. 1.

2.1 Fluid flow equations

The flow of viscous fluid through a porous elastic solid is governed by Darcy's law. The present theory is based on the following assumptions: (1) In-plane fluid velocity gradients in the shells are small compared to the transverse fluid-velocity gradient. (2) The contained fluid in pore is assumed to be incompressible. The fluid flow equation is given as follows:

$$\left.\begin{aligned}&K\frac{\partial^2}{\partial\zeta^2}(\Delta P_f)=\frac{\partial}{\partial t}(\Delta P_f)\\&\quad+C\frac{\partial}{\partial t}\left\{\left(\frac{\Delta\varepsilon_{\xi m}}{L_\xi}+\frac{\Delta\varepsilon_{\theta m}}{L_\theta}\right)+\zeta\left(\frac{\Delta\kappa_\xi}{L_\xi}+\frac{\Delta\kappa_\theta}{L_\theta}\right)\right\},\\&L_\xi=1+\zeta/R_s,\ L_\theta=1+\zeta/R_\theta,\\&C=\alpha B/\beta,\ K=k/(\beta\mu_f),\\&\beta=\frac{\alpha^2}{\lambda_r+2\mu_r}+\frac{1}{M_c},\ k=\frac{1}{8}fr_p^2,\\&B=\frac{2\mu_r}{\lambda_r+2\mu_r}=\frac{1-2\nu}{1-\nu},\\&\alpha=1-\frac{C_m}{C_p},\ M_c=\frac{1}{C_m(\alpha-f)},\end{aligned}\right\}\qquad(2)$$

where P_f: fluid (pore) pressure, K: effective shell permeability, C: material parameter, k: intrinsic permeability, λ_r,μ_r: Lamẽ constants for the solid skeleton, C_m: compressibility of the material making up the skeleton, C_p: compressibility of the porous body, μ_f: fluid viscosity, r_p: void radius, f: porosity, ν: Poisson's ratio, α: constant determined from compressibility, $\varepsilon_{\xi m}$, $\varepsilon_{\theta m}$: strains of the middle surface, κ_ξ, κ_θ: bending distortions, Δ: refers to increment, t: time.

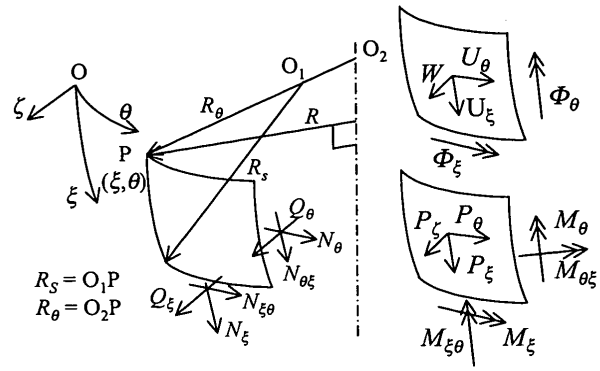

Fig. 1 Coordinates and notations

The boundary conditions of the fluid pressure on the inner and outer surfaces $(\zeta=\mp h/2)$ of the shell are

$\zeta=-h/2$:

$\Delta P_f=\Delta P_{\rm in}$ (on a permeable surface),

$\partial(\Delta P_f)/\partial\zeta=0$ (on a impermeable surface),

$\zeta=h/2$:

$\Delta P_f=-\Delta P_{\rm out}$ (on a permeable surface),

$\partial(\Delta P_f)/\partial\zeta=0$ (on a impermeable surface),

where h is the thickness of the shell, and $P_{\rm in}$, $P_{\rm out}$ are internal and external pressures, respectively.

2.2 Deformation equations

Adding the inertia terms to the equilibrium equations in the Reissner shell theory[9] and applying these to the shells of revolution, the following equations of motion expressed in the incremental forms are obtained, where the rotatory inertia terms are omitted:

$$\left.\begin{aligned}&\frac{\partial}{\partial\xi}(\Delta N_\xi)+\gamma(\Delta N_\xi-\Delta N_\theta)+\frac{1}{r}\frac{\partial}{\partial\theta}(\Delta N_{\theta\xi})+\omega_\xi\Delta Q_\xi+a\left[\Delta P_\xi-\rho h\frac{\partial^2}{\partial t^2}(\Delta U_\xi)\right]=0,\\&\frac{\partial}{\partial\xi}(\Delta N_{\xi\theta})+\gamma(\Delta N_{\xi\theta}+\Delta N_{\theta\xi})+\frac{1}{r}\frac{\partial}{\partial\theta}(\Delta N_\theta)+\omega_\theta\Delta Q_\theta+a\left[\Delta P_\theta-\rho h\frac{\partial^2}{\partial t^2}(\Delta U_\theta)\right]=0,\\&\frac{\partial}{\partial\xi}(\Delta Q_\xi)+\gamma\Delta Q_\xi+\frac{1}{r}\frac{\partial}{\partial\theta}(\Delta Q_\theta)-(\omega_\xi\Delta N_\xi+\omega_\theta\Delta N_\theta)+a\left[\Delta P_\zeta-\rho h\frac{\partial^2}{\partial t^2}(\Delta W)\right]=0,\\&\Delta Q_\xi-\frac{1}{a}\left[\frac{\partial}{\partial\xi}(\Delta M_\xi)+\gamma(\Delta M_\xi-\Delta M_\theta)+\frac{1}{r}\frac{\partial}{\partial\theta}(\Delta M_{\theta\xi})\right]=0,\\&\Delta Q_\theta-\frac{1}{a}\left[\frac{\partial}{\partial\xi}(\Delta M_{\xi\theta})+\gamma(\Delta M_{\xi\theta}+\Delta M_{\theta\xi})+\frac{1}{r}\frac{\partial}{\partial\theta}(\Delta M_\theta)\right]=0.\end{aligned}\right\}\qquad(3)$$

The notation ρ in the inertia terms is mass density for the shells, and the other variables are shown in Fig. 1. P_ξ, P_θ and P_ζ in Fig. 1 are components of distributed loads per unit area of the middle surface, and those are connected with internal loads $\{P_\xi^-, P_\theta^-, P_\zeta^-\}$ and external loads $\{P_\xi^+, P_\theta^+, P_\zeta^+\}$ by following relation:

$$\{P_\xi, P_\theta, P_\zeta\}=\{P_\xi^-, P_\theta^-, P_\zeta^-\}h^- - \{P_\xi^+, P_\theta^+, P_\zeta^+\}h^+, \tag{4}$$

where

$$h^\pm = 1 \pm \frac{h}{2}\left(\frac{1}{R_s}+\frac{1}{R_\theta}\right)+\frac{h^2}{4}\frac{1}{R_sR_\theta}. \tag{5}$$

The strains of the middle surface are given by the displacements U_ξ, U_θ, W in the next equations[10]:

$$\left.\begin{aligned}&\Delta\varepsilon_{\xi m}=\frac{1}{a}\left[\frac{\partial}{\partial\xi}(\Delta U_\xi)+\omega_\xi\Delta W\right],\ \Delta\varepsilon_{\theta m}=\frac{1}{a}\left[\frac{1}{r}\frac{\partial}{\partial\theta}(\Delta U_\theta)+\gamma\Delta U_\xi+\omega_\theta\Delta W\right],\\&\Delta\varepsilon_{\xi\theta m}=\frac{1}{2a}\left[\frac{1}{r}\frac{\partial}{\partial\theta}(\Delta U_\xi)+\frac{\partial}{\partial\xi}(\Delta U_\theta)-\gamma\Delta U_\theta\right],\end{aligned}\right\} \tag{6}$$

where $\varepsilon_{\xi\theta m}$ is half the usual engineering shear strain.

The relations between the bending distortions $\varkappa_\xi$, $\varkappa_\theta$, $\varkappa_{\xi\theta}$, $\varkappa_{\theta\xi}$ and the displacements are[10]

$$\left.\begin{aligned}&\Delta\varkappa_\xi=\frac{1}{a}\frac{\partial}{\partial\xi}(\Delta\Phi_\xi),\ \Delta\varkappa_\theta=\frac{1}{a}\left[\frac{1}{r}\frac{\partial}{\partial\theta}(\Delta\Phi_\theta)+\gamma\Delta\Phi_\xi\right],\\&\Delta\varkappa_{\xi\theta}=\frac{1}{2a}\left[\frac{\partial}{\partial\xi}(\Delta\Phi_\theta)-2\omega_\xi\Delta\Phi_n\right],\ \Delta\varkappa_{\theta\xi}=\frac{1}{2a}\left[\frac{1}{r}\frac{\partial}{\partial\theta}(\Delta\Phi_\xi)-\gamma\Delta\Phi_\theta+2\omega_\theta\Delta\Phi_n\right],\end{aligned}\right\} \tag{7}$$

where rotations Φ_ξ, Φ_θ and Φ_n are

$$\left.\begin{aligned}&\Delta\Phi_\xi=\frac{1}{a}\left[-\frac{\partial}{\partial\xi}(\Delta W)+\omega_\xi\Delta U_\xi\right]+2\Delta\varepsilon_{\xi\zeta m},\\&\Delta\Phi_\theta=\frac{1}{a}\left[-\frac{1}{r}\frac{\partial}{\partial\theta}(\Delta W)+\omega_\theta\Delta U_\theta\right]+2\Delta\varepsilon_{\theta\zeta m},\\&\Delta\Phi_n=\frac{1}{2a}\left[-\frac{1}{r}\frac{\partial}{\partial\theta}(\Delta U_\xi)+\frac{1}{\partial\xi}(\Delta U_\theta)+\gamma\Delta U_\theta\right].\end{aligned}\right\} \tag{8}$$

The strain components at a distance ζ from the middle surface are given as

$$\left.\begin{aligned}&\Delta\varepsilon_\xi=(\Delta\varepsilon_{\xi m}+\zeta\Delta\varkappa_\xi)/L_\xi,\ \Delta\varepsilon_\theta=(\Delta\varepsilon_{\theta m}+\zeta\Delta\varkappa_\theta)/L_\theta,\\&\Delta\varepsilon_{\xi\theta}=\left[\frac{1}{2}(\Delta\varepsilon_{\xi\theta m}+\Delta\Phi_n)+\zeta\left(\Delta\varkappa_{\xi\theta}+\frac{\omega_\xi}{a}\Delta\Phi_n\right)\right]\Big/L_\xi\\&\quad+\left[\frac{1}{2}(\Delta\varepsilon_{\xi\theta m}-\Delta\Phi_n)+\zeta\left(\Delta\varkappa_{\theta\xi}-\frac{\omega_\theta}{a}\Delta\Phi_n\right)\right]\Big/L_\theta,\\&\Delta\varepsilon_{\xi\zeta}=\Delta\varepsilon_{\xi\zeta m}/L_\xi,\ \Delta\varepsilon_{\theta\zeta}=\Delta\varepsilon_{\theta\zeta m}/L_\theta.\end{aligned}\right\} \tag{9}$$

As the constitutive relations, we shall use Biot's consolidation theory[11],[12] for poroelastic solids. In the present theory where the stress component σ_ζ normal to the middle surface can be assumed to be negligible, the relations between the total stresses per unit area of bulk material and the fluid (pore) pressure are

$$\left.\begin{aligned}&\Delta\sigma_\xi=\frac{E}{1-\nu^2}(\Delta\varepsilon_\xi+\nu\Delta\varepsilon_\theta)-B\alpha\Delta P_f,\ \Delta\sigma_\theta=\frac{E}{1-\nu^2}(\Delta\varepsilon_\theta+\nu\Delta\varepsilon_\xi)-B\alpha\Delta P_f,\\&\Delta\sigma_{\xi\theta}=\frac{E}{1+\nu}\Delta\varepsilon_{\xi\theta},\ \Delta\sigma_{\xi\zeta}=\frac{E}{1+\nu}\Delta\varepsilon_{\xi\zeta},\ \Delta\sigma_{\theta\zeta}=\frac{E}{1+\nu}\Delta\varepsilon_{\theta\zeta},\\&\Delta P_f=M_c(\Delta\zeta_f-\alpha\Delta\varepsilon),\ \Delta\zeta_f=(\Delta\varepsilon-\Delta\varepsilon_f)f,\end{aligned}\right\} \tag{10}$$

where ε and ε_f are the solid and fluid dilatations, respectively. ζ_f is the fluid filtration, and E is the Young's modulus for the drained solid skeleton.

By the use of Eqs. (9) and (10) with the following approximations

$$\left.\begin{aligned}&\int_{-h/2}^{h/2}L_\theta/L_\xi d\zeta\cong h\left[1+\frac{h^2}{12R_s}\left(\frac{1}{R_s}-\frac{1}{R_\theta}\right)\right],\ \int_{-h/2}^{h/2}L_\theta/L_\xi\zeta d\zeta\cong-\frac{h^3}{12}\left[\frac{1}{R_s}-\frac{1}{R_\theta}\right],\\&\int_{-h/2}^{h/2}L_\theta/L_\xi\zeta^2 d\zeta\cong\frac{h^3}{12}\left[1+\frac{3}{20}\frac{h^2}{R_s}\left(\frac{1}{R_s}-\frac{1}{R_\theta}\right)\right],\end{aligned}\right\} \tag{11}$$

the resultant stresses and the resultant moments per unit length are

$$\left.\begin{aligned}&\Delta N_\xi=\left\{\int_{-h/2}^{h/2}Ed\zeta/(1-\nu^2)\right\}\left[\Delta\varepsilon_{\xi m}+\nu\Delta\varepsilon_{\theta m}-\frac{h^2}{12a}(\omega_\xi-\omega_\theta)\Delta\varkappa_\xi\right]-B\alpha\Delta N_{f\xi},\\&\Delta N_{\xi\theta}=\left\{\int_{-h/2}^{h/2}Ed\zeta/(1+\nu)\right\}\left[\Delta\varepsilon_{\xi\theta m}+\frac{h^2}{12a}(\omega_\xi-\omega_\theta)\left\{\frac{1}{2R_s}(\Delta\varepsilon_{\xi\theta m}-\Delta\Phi_n)-\Delta\varkappa_{\xi\theta}\right\}\right],\\&\Delta Q_\xi=\frac{5}{6}\left\{\int_{-h/2}^{h/2}Ed\zeta/(1+\nu)\right\}\Delta\varepsilon_{\xi\zeta m},\\&\Delta M_\xi=\left\{\int_{-h/2}^{h/2}E\zeta^2 d\zeta/(1-\nu^2)\right\}\left[\Delta\varkappa_\xi+\nu\Delta\varkappa_\theta-\frac{1}{a}(\omega_\xi-\omega_\theta)\Delta\varepsilon_{\xi m}\right]-B\alpha\Delta M_{f\xi},\\&\Delta M_{\xi\theta}=\left\{\int_{-h/2}^{h/2}E\zeta^2 d\zeta/(1+\nu)\right\}\left[\Delta\varkappa_{\xi\theta}+\Delta\varkappa_{\theta\xi}-\frac{1}{2a}(\omega_\theta-\omega_\xi)(\Delta\Phi_n-\Delta\varepsilon_{\xi\theta m})\right],\end{aligned}\right\} \tag{12}$$

where $N_{f\xi}$, $M_{f\xi}$ are the force and moment resultants due to pore pressure across the shell thickness, respectively, and are given by

$$\{\Delta N_{f\xi}, \Delta M_{f\xi}\}=\int_{-h/2}^{h/2}\{\Delta P_f, \zeta\Delta P_f\}L_\theta d\zeta. \tag{13}$$

Furthermore, ΔN_θ, $\Delta N_{\theta\xi}$, ΔQ_θ, ΔM_θ, $\Delta M_{\theta\xi}$ and $\Delta N_{f\theta}$, $\Delta M_{f\theta}$ are obtained by exchanging the subscripts ξ and θ in equations for ΔN_ξ, $\Delta N_{\xi\theta}$, ΔQ_ξ, ΔM_ξ, $\Delta M_{\xi\theta}$ and $\Delta N_{f\xi}$, $\Delta M_{f\xi}$ and by changing the sign of $\Delta\Phi_n$.

A complete set of field equations for 35 independent variables; ΔN_ξ, ΔN_θ, $\Delta N_{\xi\theta}$, $\Delta N_{\theta\xi}$, ΔQ_ξ, ΔQ_θ, ΔM_ξ, ΔM_θ, $\Delta M_{\xi\theta}$, $\Delta M_{\theta\xi}$, $\Delta N_{f\xi}$, $\Delta N_{f\theta}$, $\Delta M_{f\xi}$, $\Delta M_{f\theta}$, ΔU_ξ, ΔU_θ, ΔW, $\Delta\Phi_\xi$, $\Delta\Phi_\theta$, $\Delta\Phi_n$, $\Delta\varepsilon_{\xi m}$, $\Delta\varepsilon_{\theta m}$, $\Delta\varepsilon_{\xi\theta m}$, $\Delta\varepsilon_{\xi\zeta m}$, $\Delta\varepsilon_{\theta\zeta m}$, $\Delta\kappa_\xi$, $\Delta\kappa_\theta$, $\Delta\kappa_{\xi\theta}$, $\Delta\kappa_{\theta\xi}$, $\Delta\sigma_\xi$, $\Delta\sigma_\theta$, $\Delta\sigma_{\xi\theta}$, $\Delta\sigma_{\xi\zeta}$, $\Delta\sigma_{\theta\zeta}$, ΔP_f is now given by 35 equations, (3), (6)~(8), (10), (12) and (13).

3. Nondimensional Equations

In order to analyze the problem of shells under arbitrary unsymmetrical loads, the 35 independent variables and the distributed loads mentioned in chapter 2 are expanded into Fourier series. Only the variables which have not been mentioned in the published paper[15] are shown as follows:

$$\{\Delta P_f, \Delta N_{f\xi}, \Delta N_{f\theta}, \Delta M_{f\xi}, \Delta M_{f\theta}\}=\sigma_0 h\sum_{n=0}^{\infty}\left\{\frac{1}{a}\Delta p_f^{(n)}, \Delta n_{f\xi}^{(n)}, \Delta n_{f\theta}^{(n)}, \frac{h^2}{a}\Delta m_{f\xi}^{(n)}, \frac{h^2}{a}\Delta m_{f\theta}^{(n)}\right\}\cos n\theta, \tag{14}$$

where corresponding small letters are adopted as the Fourier coefficients, and σ_0 is a reference stress.

Substituting these Fourier series into the above fundamental equations, the equations among the Fourier coefficients relating to the variables are obtained. From the fluid flow equation the following nondimensional equation is obtained:

$$\frac{\partial^2(\Delta p_f^{(n)})}{\partial(\zeta/h)^2}=\frac{h^2}{aK}\sqrt{\frac{E}{\rho}}\left[\Delta\dot{p}_f^{(n)}+\frac{aC}{Eh}\left\{\left(\frac{\Delta\dot{e}_{\xi m}^{(n)}}{L_\xi}+\frac{\Delta\dot{e}_{\theta m}^{(n)}}{L_\theta}\right)+\frac{\zeta}{a}\left(\frac{\Delta\dot{\kappa}_\xi^{(n)}}{L_\xi}+\frac{\Delta\dot{\kappa}_\theta^{(n)}}{L_\theta}\right)\right\}\right]. \tag{15}$$

Similarly eliminating the variables from the deformation equations, the second simultaneous differential equations for the displacement increments $\Delta u_\xi^{(n)}$, $\Delta u_\theta^{(n)}$, $\Delta w^{(n)}$ and the rotational increments $\Delta\phi_\xi^{(n)}$, $\Delta\phi_\theta^{(n)}$ can be derived as

$$A_1\{Z\}''+A_2\{Z\}'+A_3\{Z\}=A_4\{N_f\}'+A_5\{N_f\}+A_6\{\ddot{Z}\}+A_7\{p\}, \tag{16}$$

where $\{Z\}=\{\Delta u_\xi^{(n)}, \Delta u_\theta^{(n)}, \Delta w^{(n)}, \Delta\phi_\xi^{(n)}, \Delta\phi_\theta^{(n)}\}^T$, $\{N_f\}=\{\Delta n_{f\xi}^{(n)}, \Delta n_{f\theta}^{(n)}, \Delta m_{f\xi}^{(n)}, \Delta m_{f\theta}^{(n)}\}^T$ and $\{p\}=\{\Delta p_\xi^{(n)}, \Delta p_\theta^{(n)}, \Delta p_\zeta^{(n)}\}^T$. Also $\{\ \}'$, $(\dot{\ })$ and $(\ddot{\ })$ denote $d(\ )/d\xi$, $\partial(\ )/\partial\tau$ and $\partial^2(\ )/\partial\tau^2$, respectively. $\tau(=(E/\rho)^{1/2}t/a)$ is nondimensional time, and $\{\ \}^T$ represents the transposed matrix. A_1~A_3 are 5×5 matrices determined from the shell form and ν, and A_4~A_7 are given as follows:

$$\left.\begin{aligned}
A_4&=\begin{bmatrix} B\alpha & 0 & 0 & 0\\ 0 & 0 & 0 & 0\\ 0 & 0 & 0 & 0\\ 0 & 0 & -\lambda^2 B\alpha & 0\\ 0 & 0 & 0 & 0\end{bmatrix},\quad A_5=\begin{bmatrix} B\alpha\gamma & -B\alpha\gamma & 0 & 0\\ 0 & -\frac{n}{\gamma}B\alpha & 0 & 0\\ -B\alpha\omega_\xi & -B\alpha\omega_\theta & 0 & 0\\ 0 & 0 & -\lambda^2\gamma B\alpha & \lambda^2\gamma B\alpha\\ 0 & 0 & 0 & \frac{n}{\gamma}\lambda^2 B\alpha\end{bmatrix},\\
A_6&=\begin{bmatrix} 1 & 0 & 0 & 0 & 0\\ 0 & 1 & 0 & 0 & 0\\ 0 & 0 & 1 & 0 & 0\\ 0 & 0 & 0 & 0 & 0\\ 0 & 0 & 0 & 0 & 0\end{bmatrix},\quad A_7=\begin{bmatrix} -1 & 0 & 0\\ 0 & -1 & 0\\ 0 & 0 & -1\\ 0 & 0 & 0\\ 0 & 0 & 0\end{bmatrix},
\end{aligned}\right\} \tag{17}$$

where $\lambda=h/a$.

4. Numerical Method

In order to solve the fluid and solid coupling equations, firstly we assume that the strain rates are zero in the fluid flow equation, and calculate the distributions of pore pressure increments under the given boundary conditions. By substitution of the obtained pore pressure increments into the shell deformation equations, the increments of displacements and strains are obtained. Then by using the obtained strain increments, the modified distributions of pore pressure increments are calculated. These procedures are continued until the pore pressure distribution is converged enough, and the increments of pore pressure, displacements, strains and stresses with respect to the time increment are decided. For the solutions of these equations a finite difference method is employed and the inertia terms are treated with the backward difference formula proposed by Houbolt[13]. The integration is carried out numerically by the use of Simpson's 1/3 rule. The solutions at any time are obtained by integration of the incremental values at each calculating stage.

5. Numerical Example

As a numerical example, the simply supported porous cylindrical shell made of silicon carbide

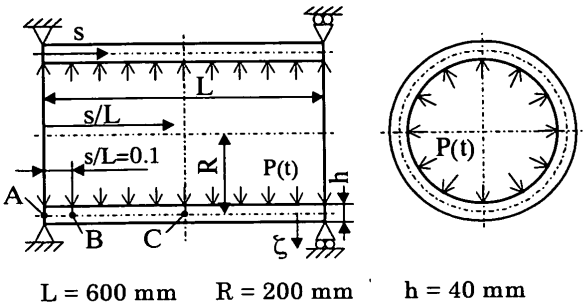

Fig. 2 Cylindrical shell

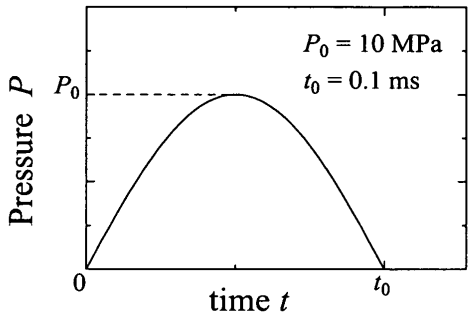

Fig. 3 Load

ceramics under a semi-sinusoidal internal load with respect to time, as shown in Figs. 2 and 3, is analyzed. Viscous fluid is saturated in the shell body, and four cases of surface boundary conditions on the permeability are examined:

Case 1: Inner and outer surfaces of the shell are both permeable.

Case 2: Inner surface is permeable, but outer surface is impermeable.

Case 3: Inner surface is impermeable, but outer surface is permeable.

Case 4: Inner and outer surfaces are both impermeable.

The geometrical parameters of the shell are as follows:

$$\left.\begin{array}{l} a=R,\ \xi=s/L,\ r=1,\ r'=0, \\ \gamma=0,\ \omega_\xi=\omega'_\xi=0,\ \omega_\theta=1. \end{array}\right\} \quad (18)$$

Boundary conditions at the points A and C are

$$\left.\begin{array}{l} \Delta U_\theta=\Delta W=\Delta\Phi_\theta=\Delta N_\xi=\Delta M_\xi=0 \\ \qquad\qquad\qquad\qquad\qquad\qquad \text{(Point A)}, \\ \Delta U_\xi=\Delta\Phi_\xi=\Delta Q_\xi=\Delta N_{\xi\theta}=\Delta M_{\xi\theta}=0 \\ \qquad\qquad\qquad\qquad\qquad\qquad \text{(Point C)}. \end{array}\right\} \quad (19)$$

On the inner and outer surfaces, the following equations are employed:

$$\left.\begin{array}{l} \text{Case 1: } \Delta P_f=\Delta P_{\text{in}},\ \Delta P_f=-\Delta P_{\text{out}}, \\ \text{Case 2: } \Delta P_f=\Delta P_{\text{in}},\ (\partial(\Delta P_f)/\partial\zeta)_{\text{out}}=0, \\ \text{Case 3: } (\partial(\Delta P_f)/\partial\zeta)_{\text{in}}=0,\ \Delta P_f=-\Delta P_{\text{out}}, \\ \text{Case 4: } (\partial(\Delta P_f)/\partial\zeta)_{\text{in}}=0,\ (\partial(\Delta P_f)/\partial\zeta)_{\text{out}}=0. \end{array}\right\} \quad (20)$$

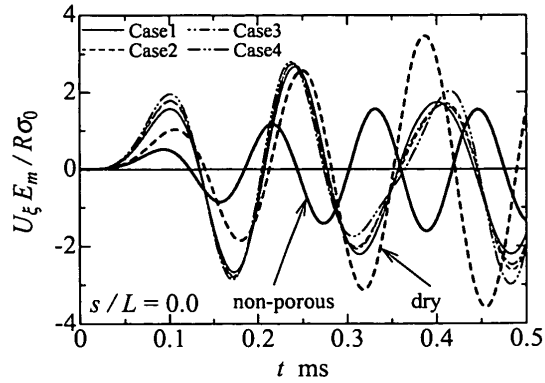

Fig. 4 Variations of U_ξ at point A with time

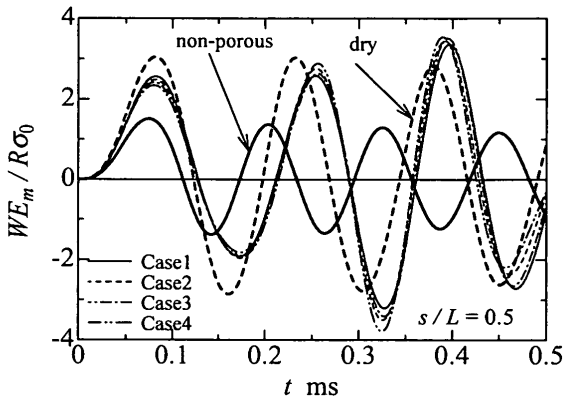

Fig. 5 Variations of W at point C with time

The meridional mesh point number is chosen to be 101, and the division number through the thickness is selected as 21. The increment of time Δt is decided as 0.1 μs. These values are obtained in consideration of convergence of the solutions.

The material constants employed in the calculation are as follows:

$$\left.\begin{array}{l} \text{Silicon carbide ceramics:} \\ \quad E_m=370\ \text{GPa},\ \rho_m=3.2\ \text{g/cm}^3, \\ \quad \nu=0.16. \\ \text{Viscous fluid:} \\ \quad \rho_f=0.85\ \text{g/cm}^3,\ \mu_f=0.2\ \text{Pa}\cdot\text{s}. \\ \text{Poroelastic solid:} \\ \quad E=E_m(1-f)^2,\ \rho=\rho_m(1-f)+\rho_f f, \\ \quad \alpha=1-C_m/C_p=1-(1-f)^2, \\ \quad f=0.3,\ r_p=5\ \mu\text{m}. \end{array}\right\} \quad (21)$$

Now we shall discuss some results of calculations. In Figs. 4~14 the solid lines, broken lines and two kinds of chain lines indicate the values for four cases of surface boundary conditions on the permeability, respectively. For the reference stress σ_0, the statical hoop stress of a cylindrical shell under inner pressure $P_0(\sigma_0=P_0R/h)$ is employed.

The variations of meridional displacement U_ξ at the simply supported edge (Point A: $s/L=0$), radial displacement W at the middle cross section (Point C:

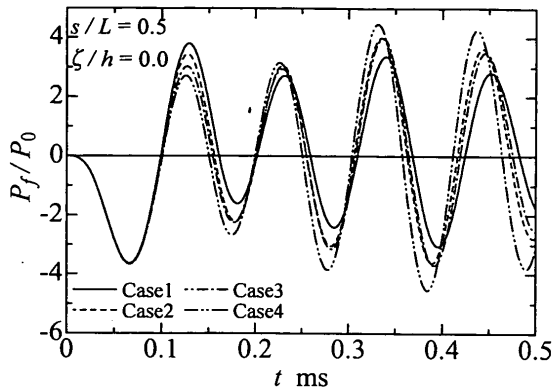

Fig. 6 Variations of P_f on the middle surface at point C with time

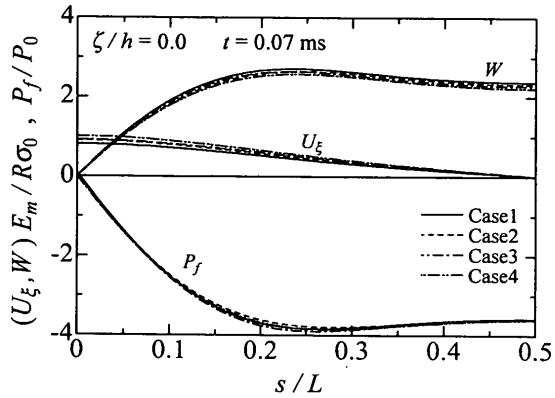

Fig. 7 Meridional distributions of U_ξ, W and P_f at $t=0.07$ ms

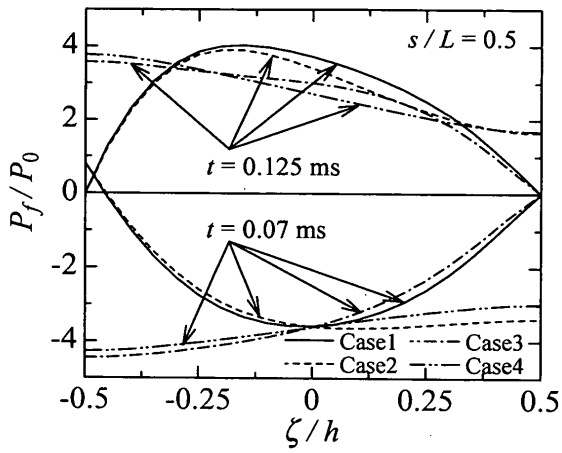

Fig. 8 Distributions of P_f through thickness at point C

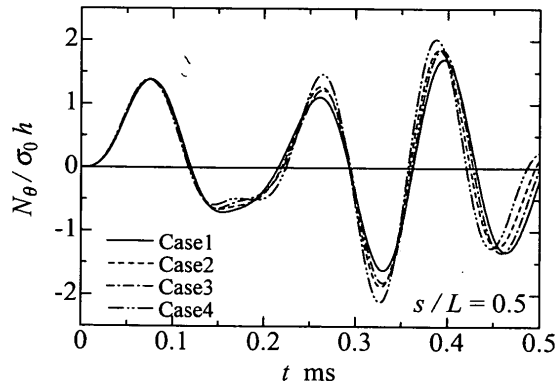

Fig. 9 Variations of N_θ at point C with time

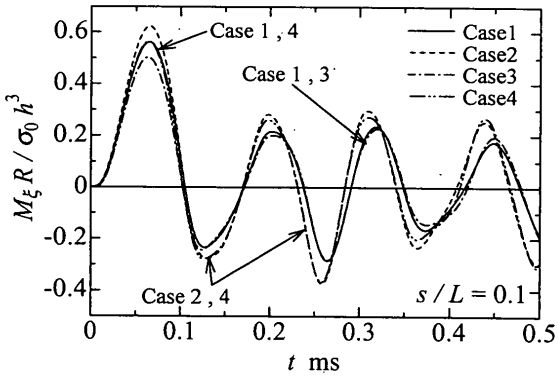

Fig. 10 Variations of M_ξ at point B with time

$s/L=0.5$) and pore pressure P_f on the middle surface at point C with time are shown in Figs. 4~6, respectively. Figure 7 illustrates the meridional distributions of U_ξ, W and P_f on the middle surface of the shell at time $t=0.07$ ms when the shell deforms largely outward firstly after loading and pore pressure at point C becomes minimum. Distributions of P_f at point C through the shell thickness at $t=0.07$ ms and 0.125 ms are also shown in Fig. 8. In Figs. 4 and 5 the results for the case of a dry shell and for a nonporous solid shell are also plotted by thick broken and solid lines, respectively. From Fig. 7 at the initial loading stage, strain becomes tensile throughout the shell with the increase of W, and owing to the expansion of pore volume in the shell body, pore pressure shows negative value. From Fig. 8 near the inner and outer surfaces of the shell, there is a remarkable difference between solutions for each surface permeability condition. In Fig. 6 this difference is also found on the middle surface of the shell, and becomes large with the lapse of time. From the variations of displacements with time (Fig. 5), it is found that in comparison with nonporous shells, displacements of the porous shells vary largely and slowly with the lapse of time, and the shells saturated in viscous fluid deform more slowly with time. The difference of displacements for each permeability condition is small in comparison with the difference of pore pressure, but tends to become large with the lapse of time.

Figures 9 and 10 show the variations of the resultant force N_θ at point C and the resultant moment M_ξ at point B ($s/L=0.1$) with time, respectively. The point B is a position where resultant moments become large for the statical load. The distributions of axial stress σ_ξ and circumferential stress σ_θ through the

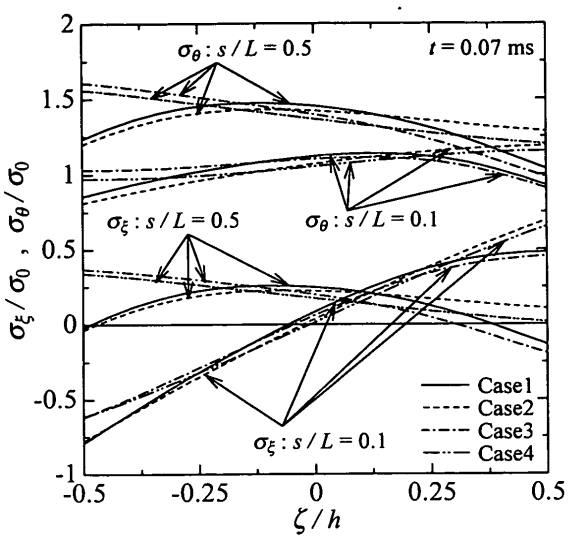

Fig. 11 Distributions of σ_ξ and σ_θ through thickness at t=0.07 ms

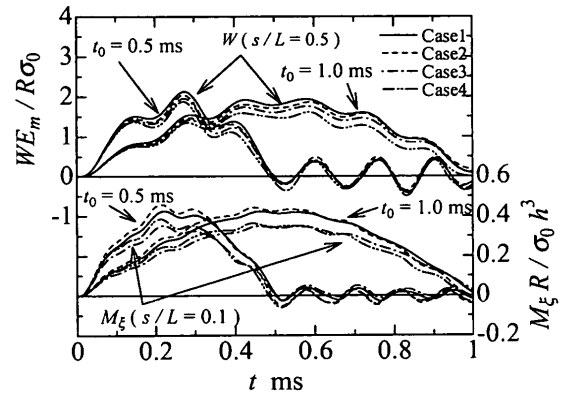

Fig. 12 Variations of W and M_ξ with time (t_0=0.5, 1.0 ms)

shell thickness at points B and C at t=0.07 ms are illustrated in Fig. 11. The distributions of P_f near the inner and outer surfaces of the shell due to the permeability as shown in Fig. 8 has effects on the stress distributions, and so on the resultant forces and resultant moments. The variations of N_θ with time are similar to the response of W, and the difference due to the boundary permeability conditions becomes large with the lapse of time. The stress distributions near the shell surfaces has a great influence on M_ξ, and the difference of M_ξ appears greatly immediately after loading.

Next we shall discuss the influence of the impulsive loading rate and the boundary permeability conditions on the inner and outer surfaces of porous shells upon the displacements and stresses. The variations of W at point C and M_ξ at point B with time for two semi-sinusoidal internal loads (continuity time t_0=0.5 ms, 1.0 ms) are shown in Fig. 12. For the case of t_0= 0.5 ms, the variations of P_f on the middle surface at

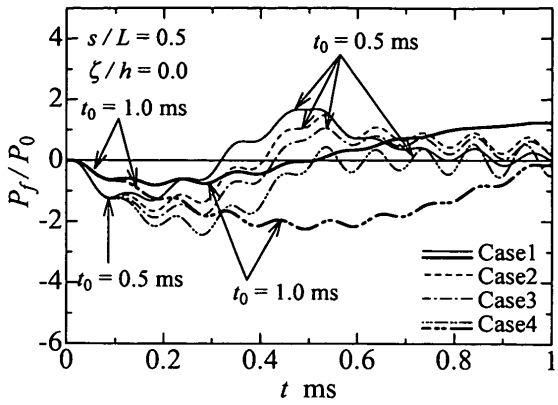

Fig. 13 Variations of P_f on the middle surface at point C with time

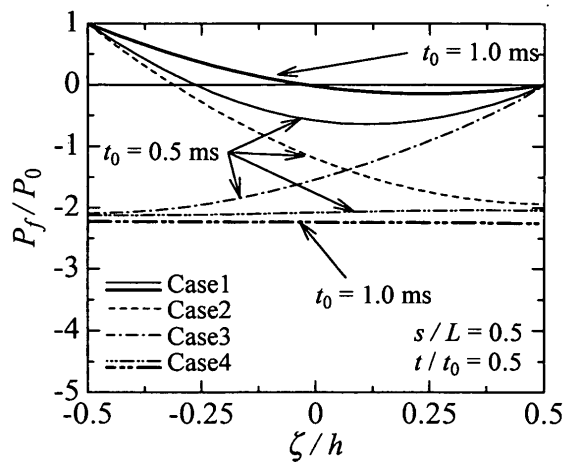

Fig. 14 Distributions of P_f through thickness at point C

point C with time and the distributions of P_f through thickness at point C at peak loading time t/t_0=0.5 are illustrated in Figs. 13 and 14, respectively. The results of case 1 and case 4 for t_0=1.0 ms are also plotted by thick lines. By comparison with the results for t_0=0.1 ms (vid. Figs. 5, 6, 8 and 10), for the lower impulsive loading rate, the difference due to the boundary permeability conditions can be seen for the loading time t_0, and especially for W, this difference becomes a little larger with the increase of t_0. The shells, whose both surfaces are permeable, are most deformed outward, and the deformation of shells whose both surfaces are impermeable is the smallest. Main cause of the different variations with time as shown in Fig. 12 is due to the difference of pore pressure distributions in the shell body (vid. Figs. 8 and 14).

Finally comparison between solutions from the present theory and the thin shell theory which neglects the effect of shear deformations for the case of t_0=0.1 ms is shown in Figs. 15 and 16. Inner and outer surfaces of the shell are assumed to be permeable (Case 1). Figure 15 shows the variations of W and P_f at point C on the middle surface with time, and Fig. 16

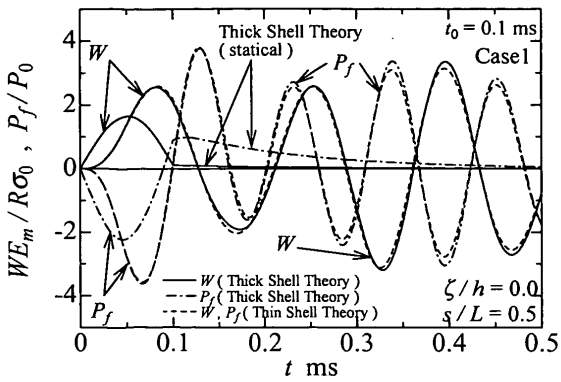

Fig. 15 Variations of W and P_f at point C with time

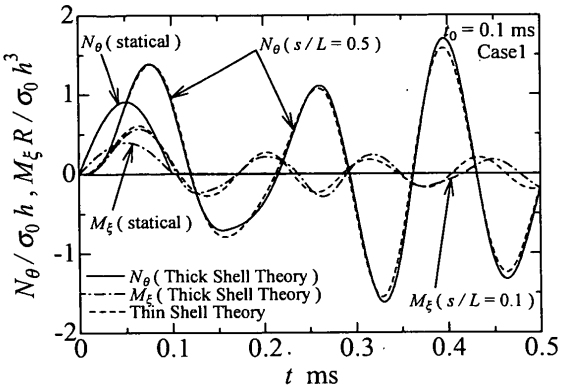

Fig. 16 Variations of N_θ at point C and M_ξ at point B with time

illustrates the variations of N_θ at point C and M_ξ at point B with time. In the present numerical example relatively thick shells, whose ratio of the shell thickness to the mean radius of curvature is about 0.2, are adopted, so that a little influence of the shear deformation is found for all components of displacements, pore pressure and internal forces. Also results from the thick shell theory which neglects the inertia term are plotted in Figs. 15 and 16. The displacements and internal forces are almost similar to the variations of semi-sinusoidal internal pressure with time until near the end of loading (0.1 ms). However, the variations of P_f on the middle surface at point C are different from other components, and due to fluid viscosity P_f decreases gradually with time after the end of loading. This phenomenon also appears a little in displacement components.

The discussions on the influences of porosity, void radius and fluid viscosity upon internal forces and displacements of the shell are omitted here on account of limited space, but these are almost the same as the solutions for thin shells[7].

6. Conclusions

In this paper we have described the numerical analysis of the elastic dynamic problems of fluid-saturated porous moderately thick shells of revolution. For the viscous fluid flow equations through porous solids Darcy's law has been used, and the equations of motion and the strain displacement relations have been derived from the Reissner-Naghdi shell theory. As the constitutive relations, the consolidation theory of Biot for models of fluid-solid mixtures has been employed. The numerical method selected for this problem is a method using finite difference in both space and time.

As a numerical example, simply supported cylindrical porous shells under semi-sinusoidal internal loads with respect to time have been analyzed, and the difference of the response for the different permeability boundary conditions on the inner and outer surfaces of shells has been discussed.

From the computations, we found the following.

(1) The boundary permeability conditions on the inner and outer surfaces of shells have a great influence on the distributions of pore pressure and stress components through shell thickness.

(2) This influence upon the displacements is small in the case of high impulsive loading rate, but for the low impulsive loading rate, this influence becomes great. The displacements of the shells whose inner and outer surfaces are both permeable become larger than those whose surfaces are impermeable.

(3) From the comparison between solutions from the present theory and the thin shell theory which neglects the effect of shear deformations, a little influence of shear deformations is found on the components of displacements and internal forces.

References

(1) Jayaraman, G., Water Transport in the Arterial Wall—A Theoretical Study, J. Biomech., Vol. 16, No. 10 (1983), pp. 833-840.

(2) Okuno, A. and Kingsbury, H.B., Dynamic Modulus of Poroelastic Materials, Trans. ASME, J. Apl. Mech., Vol. 56 (1989), pp. 535-540.

(3) Taber, L.A., A Theory for Transverse Deflection of Poroelastic Plates, Trans. ASME, J. Apl. Mech., Vol. 59 (1992), pp. 628-634.

(4) Taber, L.A., Axisymmetric Deformation of Poroelastic Shells of Revolution, Int. J. Solids and Structures, Vol. 29 (1992), pp. 3125-3143.

(5) Kurashige, M., Transient Response of a Fluid-Saturated Poroelastic Layer Subjected to a Sudden Fluid Pressure Rise, Trans. ASME, J. Apl. Mech., Vol. 49 (1982), pp. 492-496.

(6) Mishima, M., Kurashige, M., Takasawa, H. and Mori, T., Analysis of Ink Flow in a Mimeograph Printer based on the Mechanics of Fluid-Filled Poroelastic Solids, Acta Mechanica, Vol. 127, No. 1/4 (1998), pp. 51-62.

(7) Takezono, S., Tao, K., Gonda, T. and Itsuzaki, H., Dynamic Stress and Deformation of Poroelastic Shells Saturated in Viscous Fluid, Trans. Jpn. Soc. Mech. Eng., (in Japanese), Vol. 66, No. 641, A (2000), pp. 164-171.

(8) Takezono, S., Tao, K. and Gonda, T., Dynamic Stress and Deformation of Multi-Layered Poroelastic Shells of Revolution Saturated in Viscous Fluid, Proc. 4th Int. Symp. Impact Eng., Vol. 2 (2001), pp. 791-796.

(9) Reissner, E., A New Derivation of the Equations for the Deformation of Elastic Shells, Am. J. Math., Vol. 63, No. 1 (1941), pp. 177-184.

(10) Naghdi, P.M., On the Theory of Thin Elastic Shells, Q. Appl. Math., Vol. 14, No. 4 (1957), pp. 369-380.

(11) Biot, M.A., General Theory of Three-Dimensional Consolidation, J. Appl. Phys., Vol. 12 (1941), pp. 155-164.

(12) Biot, M.A. and Willis, D.G., The Elastic Coefficients of the Theory of Consolidation, J. Appl. Mech., Vol. 24 (1957), pp. 594-601.

(13) Houbolt, J.C., A Recurrence Matrix Solution for the Dynamic Response of Elastic Aircraft, J. Aeronaut. Sci. Vol. 17 (1950), pp. 540-550.

(14) Sanders, Jr., J.L., An Improved First-Approximation Theory for Thin Shells, NASA Report R-24 (1959), pp. 1-11.

(15) Takezono, S., Tao, K. and Tani, K., Elasto/Visco-Plastic Deformation of Multi-Layered Moderately Thick Shells of Revolution, JSME Int. J., Ser. 1, Vol. 34, No. 1 (1991), pp. 13-22.